SCIENCE ● ENVIRONMENT ● SOLUTIONS

Letter Report

Update of Tritium Transport Calculations for the Rulison Site: Report of Activities and Results During 2009 - 2010

prepared by

Clay A. Cooper, Jenny B. Chapman, Yong Zhang
(Desert Research Institute, Nevada System of Higher Education)

Rex Hodges (Stoller-Grand Junction)

Ming Ye (Florida State University)

submitted to

S.M. Stoller Corporation
Office of Legacy Management
U.S. Department of Energy
Grand Junction, Colorado

September 2010

The work upon which this report is based was supported by the U.S. Department of Energy under Contract #DE-AC52-06NA26383. Approved for public release; further dissemination unlimited.

THIS PAGE INTENTIONALLY LEFT BLANK

CONTENTS

LIST OF FIGURES iv
LIST OF TABLES iv
INTRODUCTION 1
RATIONALE FOR THIS REPORT 3
NEW DATA PERTINENT TO THE RULISON MODEL 3
Evaluation and Adjustment of Model Parameters and Processes 7
Nuclear and Hydraulic Fracture Geometry 7
Relative Permeability and Capillary Pressure Functions 8
Tritiated Water Partitioning Between Liquid and Gas 10
FLOW MODEL CALIBRATION 12
SUMMARY OF MODIFICATIONS TO THE RULISON FLOW AND TRANSPORT MODEL 15
MODEL RESULTS 16
Results of Tritium Migration under Existing Conditions 16
Results of Future Hypothetical Gas Production 16
SUMMARY AND DISCUSSION 22
REFERENCES 23

LIST OF FIGURES

1. Histogram of fraction of Lithology 1 identified in Noble wells located on Battlement Mesa in sections 26, 35, and 36, from the top of continuous gas to the base of the Cameo Coal. 4
2. One realization of the sandstone-shale lithologic model generated using the T-PROGS program and conditioned on the two well logs from Rulison. 5
3. Vertical slices of the lithology for the 12 realizations. 6
4. Plan view of the computational domain with nuclear chimney, chimney fractures, and inner and outer ellipsoidal fracture continua. 8
5. Capillary pressure (a), and relative permeability to liquid and gas (b) for the shale, chimney, and sandstone. 10
6. Measurements of tritiated water in liquid and vapor phases, measured during Rulison production testing. 12
7. Simulated history match of pressure, for one permeability realization, compared to data from the 1970 production test. 14
8. Mass fraction of tritiated water vapor in five-year increments for 41 years following the nuclear detonation for realization 1. 17
9. Tritiated water vapor 75 years after the nuclear detonation for (a) diffusion only (i.e., no gas production), and (b) for an initial condition three times the value used in the reference simulations. 18
10. Total pressure field (in megapascals) after 30 years of gas production for all 12 permeability/porosity realizations. 19
11. Gas production rate during 30-year period, between 41 and 71 years after the detonation, for all 12 permeability realizations. 20
12. Mass fraction of tritiated water vapor after 30 years of gas production from the well, for all 12 realizations.. 21

LIST OF TABLES

1. Input data for the simulations. 9

INTRODUCTION

Rulison is the site of an underground nuclear test conducted in west-central Colorado in 1969 with the purpose of investigating the feasibility of using nuclear explosives to stimulate production from low-permeability natural gas reservoirs. The detonation occurred 2,568 m (8,426 ft) below ground surface, creating a rubblized chimney estimated to have a diameter of 46 m (152 ft) and height of 84 m (274 ft) above the detonation point. Production testing from the chimney removed significant amounts of radionuclides from the subsurface, but radioactive contamination remains in the deep subsurface at the site. The Department of Energy Office of Legacy Management (DOE-OLM) manages the Rulison site to ensure that conditions are protective of human health and the environment. Management follows a multi-pronged approach of monitoring, institutional controls, and modeling to predict contaminant behavior. A process of continual improvement is embraced whereby new information is used to periodically update model predictions, which in turn inform monitoring and institutional controls. This report presents model updates and assessments occurring during 2009 and early 2010.

A thorough explanation of the Rulison conceptual and numerical model of subsurface radionuclide transport can be found in Cooper *et al*. (2007). It includes discussion of the explosion phenomenology and its relationship to radionuclide transport, the geologic model of the natural gas reservoir in which the nuclear detonation took place, physical and chemical principles associated with the flow and transport of tritiated radioactive gas, the implementation of those concepts into a flow and transport simulator, all input data (including the development of random permeability and porosity fields), and the results of the computer simulations. The simulations estimated the transport of tritium (as tritiated water) for a period of 38 years following the detonation in September 1969 through 2007, followed by a hypothetical 30-yr period of gas production from a gas well located 258 m (846 ft) from the detonation. The main findings were that tritium is likely to be confined within lot 11, which is the geographic unit in which DOE-OLM has an institutional control, and that during the 30-yr period of gas production, tritium reached the production well in fewer than five percent of the computer simulations. (Each simulation had a unique permeability and porosity arrangement based upon an estimated percentage of sandstone and shale in the producing formation.) In the few realizations in which tritium reached the hypothetical well, the peak concentration of gas reaching the production interval was of low enough concentration that it is likely to be of no risk to human health and the environment.

An addendum to the 2007 report (Cooper *et al*., 2009) was prepared largely as a result of peer review comments on the original report. It includes enhancements made to the model as an outgrowth of the reviews, as well as explorations of some of the assumptions. The first enhancement was to better determine the ratio by which THO partitions between the gas and aqueous phases. At equilibrium in a reservoir composed of two phases, the concentration of tritiated water will be greater in the aqueous phase, based upon thermodynamic principles. The ratio at which it partitions between the phases, however, is strongly a function of the temperature range measured in the reservoir and estimated for the chimney, as was shown in the addendum. The partitioning coefficient used in Cooper *et al.* (2007) was found to be inappropriate because it represents partitioning at a temperature of 300 °C, which is greater than the temperature encountered in the Rulison subsurface. As a result, tritium migration is overestimated in the Cooper *et al.* (2007) simulations. Temperatures in the nuclear chimney were estimated as high as

230 °C during production testing within one year after the nuclear test, while ambient reservoir temperature was recorded as 101°C. The chimney temperature was estimated based upon a 226 °C measurement 105 m above the detonation point. Using a partitioning coefficient for the ambient reservoir temperature favors tritiated water in the relatively immobile liquid phase and severely limits migration away from the nuclear chimney. Applying a partitioning coefficient for 230 °C allows greater tritium migration, but still significantly less than presented in Cooper *et al.* (2007). However, a 230 °C-based coefficient greatly overestimates vapor-phase tritium, and thus transport, in the cooler formation outside of the chimney. While the coefficient for 101°C is most appropriate for the majority of the pathway, the addendum used the coefficient for 230 °C for its sensitivity analyses because the influence of other parameters is more readily seen when some transport occurs.

The second enhancement reported in the addendum was the value used to describe tortuosity in the sandstone and shale. Molecular diffusion in porous media and fractures is retarded by a term that is the product of tortuosity and porosity on the free-air diffusion coefficient (the value for diffusion in purely gas systems with no sand grains) and accounts for the longer travel distance of gas-phase components and aqueous-phase solutes, such as THO, traveling through the network of pores. The 2007 report used a saturation-based tortuosity value, which resulted in possibly unrealistic low rates of THO diffusion in either phase. Justification for a larger tortuosity value, and hence constant diffusion coefficient, was made in the addendum.

Finally, the third enhancement included in the addendum was the manner in which porosity (volume of void space to total volume of rock) was handled in the hydraulic fractures surrounding the production interval of the hypothetical well. When gas is produced from low-permeability formations, the rocks are fractured mechanically around the borehole to increase permeability and enhance production. In the 2007 report, the hydraulically fractured media was assigned a porosity of 0.10, which is at the upper end of the porosity distribution used for the sandstone. In the addendum, this was changed so that the porosity remained the same as the value selected from the porosity distribution for the native sandstone in each realization, effectively assuming that hydraulic fractures have no effect on porosity, only on permeability. This lower porosity favors transport as it increases fluid velocity. It is important to remember, however, that flow is not described explicitly through individual fractures and their networks in the model. Rather, the fractured media is replaced by a representative continuum (an equivalent porous medium, or EPM) in which spatially defined values of permeability and porosity have been assigned.

The addendum concluded with several recommendations for investigations that could lower uncertainty in the model and increase confidence in the results. Included in these were the incorporation of information regarding sandstone and shale geometry from new wells nearby, improvement of the treatment of capillary pressure and relative permeability in the various lithologic units represented in the model, simulation of gas production using defined pressures rather than defined production rates, and a modification to the computer program to allow for temperature-dependent partitioning of tritium between phases. The importance of temperature-dependent partitioning is that most of the simulations reported here were nonisothermal; in contrast, most of the simulations in the 2007 report and all of the simulations in the 2009 addendum assumed constant temperature throughout the flow domain. Work on these and other enhancements was conducted in 2009 and early 2010 and is reported here. This report is not intended as a stand-alone document; rather it is a continuation of the results presented in the

above-cited reports (Cooper *et al*., 2007; 2009). In this update, only specific model enhancements are presented in detail and the reader is referred to the previous work for other model information.

RATIONALE FOR THIS REPORT

There are four objectives of this model update: (1) to incorporate new data acquired near the Rulison site, (2) to improve treatment of significant processes and parameters consistent with ongoing enhancements in the conceptual model, (3) to calibrate the model using historic site data, and (4) to assess the impact of these enhancements on predictions of tritium transport at the site. Increased realism in the model results and increased confidence in the results are both considered to provide value as DOE-OLM manages the site for protection of human health and the environment.

The first section following this introduction describes data collected from new gas exploration wells drilled on Battlement Mesa regarding stratigraphy in the Williams Fork reservoir. This information is compared to outcrop studies in the Piceance Basin and site-specific data from Rulison. Improvement to the hydrostratigraphic model of the site is then presented.

The next section describes several investigations into processes and parameters important to the conceptual model. Geometry of the nuclear-generated fractures and future hydraulic fractures from hypothetical production wells are examined in light of the regional stress field and revised for the model. The relative permeability and capillary pressure functions for the chimney and fracture continua were updated to reflect more appropriate relationships of pressure and permeability as a function of liquid saturation for those rock types. The model domain was extended to allow for longer fracture continua at the hypothetical production well. Finally, the TOUGH2 computer program was modified to allow partitioning of tritium between the gas and liquid phases as a function of temperature, which is critical to correctly estimating phase concentrations everywhere in the reservoir.

Calibration of the flow model is then described. This calibration uses measured values of formation pressure and flow rate acquired during production testing from the Rulison chimney. The calibration resulted in formation permeability and porosity values within the distribution of values used in the earlier Monte Carlo models and provided confidence for switching from those wide distributions to a single calibrated parameter.

After describing these various investigations and resulting model enhancements, the impact on contaminant flow and transport is assessed. First, tritium migration is simulated without nearby gas production, to estimate the current extent of contamination. Second, the impact of a hypothetical production well on the tritium distribution is simulated.

NEW DATA PERTINENT TO THE RULISON MODEL

An important aspect of the Rulison conceptual model is the depiction of the natural gas reservoir within the Williams Fork Formation. Given the highly heterogeneous nature of the fluvial deposit and the limitation of subsurface observations to boreholes, conditional random realizations of the sandstone geometry were generated for the model using probability distributions of several parameters and a program named T-PROGS (Carle, 1999). The values used in the 2007 model and addendum are as follows:

- There are two rock types: sandstone and shale.

- The volumetric proportions in the domain are 49% sandstone and 51% shale.
- Mean thickness of sandstone units is 7.5 m (vertical discretization in the model is limited to 5 m)
- Mean width of sandstone bodies is 161.1 m (horizontal discretization is limited to 20 m)
- Sandstone width and length are assumed equal

Recently acquired information from wells drilled by Noble on Battlement Mesa in sections 26, 35, and 36, indicates that Noble identifies three sandstone types based on volume percent of clay, along with shale and coal. "Lithology 1" sandstone, with a clay volume less than 12%, is apparently the only rock considered an economic reservoir. In 14 wells, the percent of Lithology1 varies from 31% to 47% of the Lower Williams Fork (from top of continuous gas to base of the Cameo), with a mean of 40% (Figure 1). This is in contrast to the 49% assumed as sandstone for the previous T-PROGS analysis. There is also a difference in the shale category, defined in the Noble well log analysis as greater than 35% clay. It accounts for only one to 12% of the section, much less than the 51% assumed in the model. The "Lithology 2" and "Lithology 3" categories are both designated as clayey sandstones that are not considered reservoir quality.

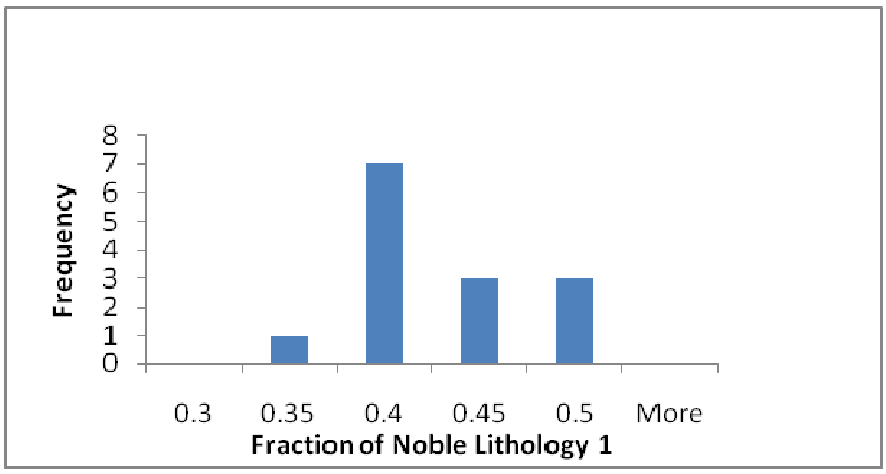

Figure 1. Histogram of fraction of Lithology 1 identified in Noble wells located on Battlement Mesa in sections 26, 35, and 36, from the top of continuous gas to the base of the Cameo Coal. Lithology 1 is defined as having less than 12% clay.

The T-PROGS model assignment was based on published information about sandstone abundance in the lower Williams Fork Formation, combined with well log analysis of the two wells at Rulison. The sandstone abundance in well RE was determined to be 48% and in well R-EX to be 59%, but both of those numbers reflect abundance in a relatively limited portion of the section near the nuclear test, and omit data from above an obvious contact between depositional facies occurring at about 2,271 m (7,450 ft) below land surface (see Figure 2-4 in Cooper *et al*., 2007). Above that contact, sandstone units are less numerous, thinner, and less continuous. Inclusion of data from above the contact in the Rulison log analysis results in sandstone percentages of 44% for A-RE and 43% for R-EX. It is likely that the log response criteria for sandstone was less strict in the 2007 model analysis, allowing more clay content, than

in Noble's assessment of the Lithology 1 reservoir type. It is also clear that the Noble Lithology 2 and Lithology 3 categories were identified as shale in the bimodal 2007 log analysis.

As the objective of the sandstone designation in the model is to represent potential gas reservoir horizons, the T-PROGS analysis is updated here with a volumetric proportion of 40% sandstone and 60% shale. This is consistent with the amount of reservoir sandstone identified in the Noble Battlement Mesa wells and also consistent with recent characterization of the lower Williams Fork as a low net-to-gross sequence with less than 50% sandstone (Cole and Cumella, 2005). The use of a lower sand percentage promotes simulated transport if the producing well and detonation are connected through high-permeability facies, though the probability of connection is decreased.

Twelve new random permeability fields were generated with the updated percentages, using the procedure outlined in Cooper *et al*. (2007). One of the conditional random fields of sandstone and shale is presented in Figure 2. Also shown is a detailed comparison of the log interpretations and the T-PROGS results at the two Rulison wells. The conditional fields can be updated as more data become available or as technological or economic conditions change what is considered reservoir-quality rock. Figure 3 shows a vertical slice from the center of the domain, in line with the location of the nuclear detonation and the production well, for all 12 realizations.

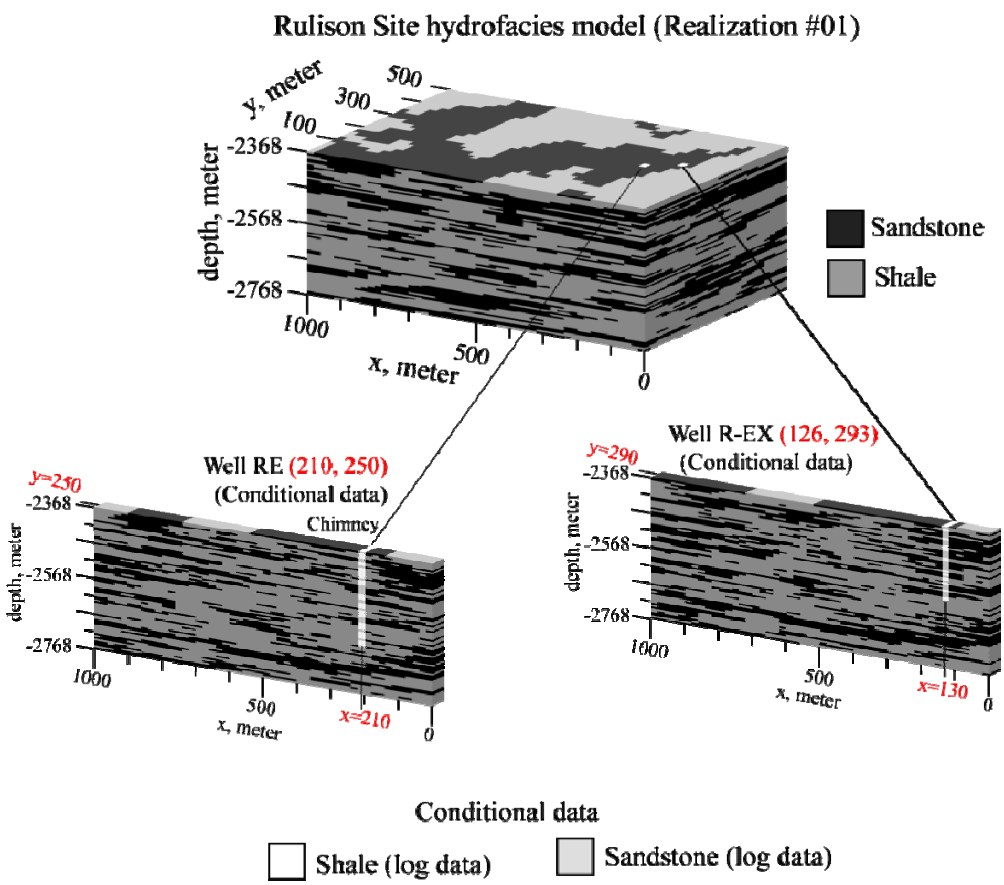

Figure 2. One realization of the sandstone-shale lithologic model generated using the T-PROGS program and conditioned on the two well logs from Rulison. The coordinates in red correspond to the location of the wells in the computational domain.

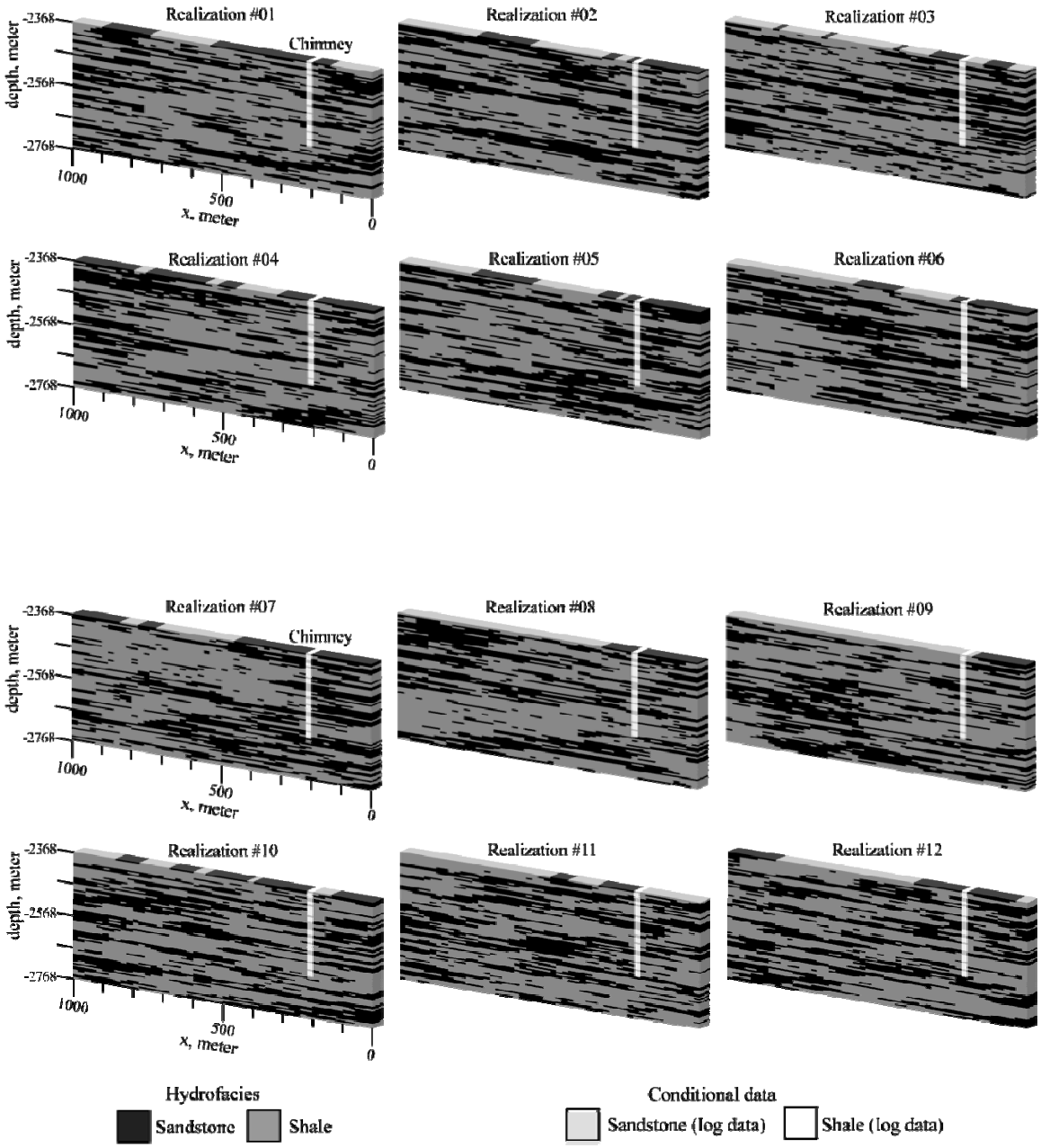

Figure 3. Vertical slices of the lithology for the 12 realizations. The slices are in the same vertical plane that contains the nuclear detonation and hypothetical production well.

Evaluation and Adjustment of Model Parameters and Processes

Three model aspects are examined in this section: the geometry of the nuclear-generated fractures and future hydraulic fractures from hypothetical production wells, the relative permeability and capillary pressure functions for the chimney and fracture continua, and the partitioning coefficient describing the amount of tritiated water in liquid and vapor form.

Nuclear and Hydraulic Fracture Geometry

The hydraulic and nuclear-stimulated fractures (fractures around the production well and chimney, respectively) in the original (Cooper *et al*., 2007) models were assumed to extend from the source of fracturing symmetrically away from the borehole in a horizontal plane. The conceptual model for these fractures is updated here to reflect that the fracture pattern may be ellipsoidal with greater extent in the direction of maximum principal stress, which is aligned east-west.

Nuclear-Generated Fractures

With respect to the nuclear-generated fracture continuum in the revised conceptual model, the ellipsoid was chosen such that the total extent in the east-west direction extends 100 m from the detonation, while the extent in the y-direction is 60 m (Figure 4). The chimney fractures extended cylindrically away from the chimney to a total distance of 80 m in the original model.

Hydraulic Fractures

The revised model specifies that the hydraulic fracture continuum extends 200 m from the perforated interval in both the east and west directions (Figure 4). In the north-south direction, the fracture continuum extends 100 m to the north and 100 m to the south from the perforated interval. The original model, in addition to extending the fractures cylindrically, treated the length of the zone of hydraulic fractures randomly; the length varied from 40 m to 160 m with a mean of 80 m (to conform to grid spacing).

The hydraulic fracture continuum is now divided into two zones. Within the inner zone, it is assumed that both sandstone and shale are hydraulically fractured, while in the outer zone it is assumed that only the sandstone is fractured. Each of these zones extends 100 m in the east-west direction. The intrinsic permeability of fractured sandstone for the two zones are assigned different values, and the intrinsic permeability of the fractured shale is assigned a value different from either of the two fractured sandstones. The values are presented in Table 1 and described below.

The properties of the EPM simulating the fracture zones are as follows: within the first 100 m of the borehole, all grid blocks (that is, both sandstone and shale) are assumed to be fractured. Within 100 meters, therefore, the fractured sandstone k_x is assigned as 4×10^{-15} m^2 while $k_{y,z}$ are assigned 4×10^{-16} m^2. For fractured shale grid blocks, $k_x = 4 \times 10^{-16}$ m^2 and $k_{y,z} = 4 \times 10^{-17}$ m^2. These values are based upon the assumption that the inner-zone fractured sandstone EPM permeability would be 100 times that of the native sandstone, and the fractured shale permeability would be ten times that of the native shale. Beyond 100 m, it is assumed that only the sandstone would be hydraulically fractured, and that the permeability of these grid blocks is ten times the native sandstone permeability. The outer fracture EPM, therefore, is assigned values $k_x = 4 \times 10^{-16}$ m^2 and $k_{y,z} = 4 \times 10^{-17}$ m^2.

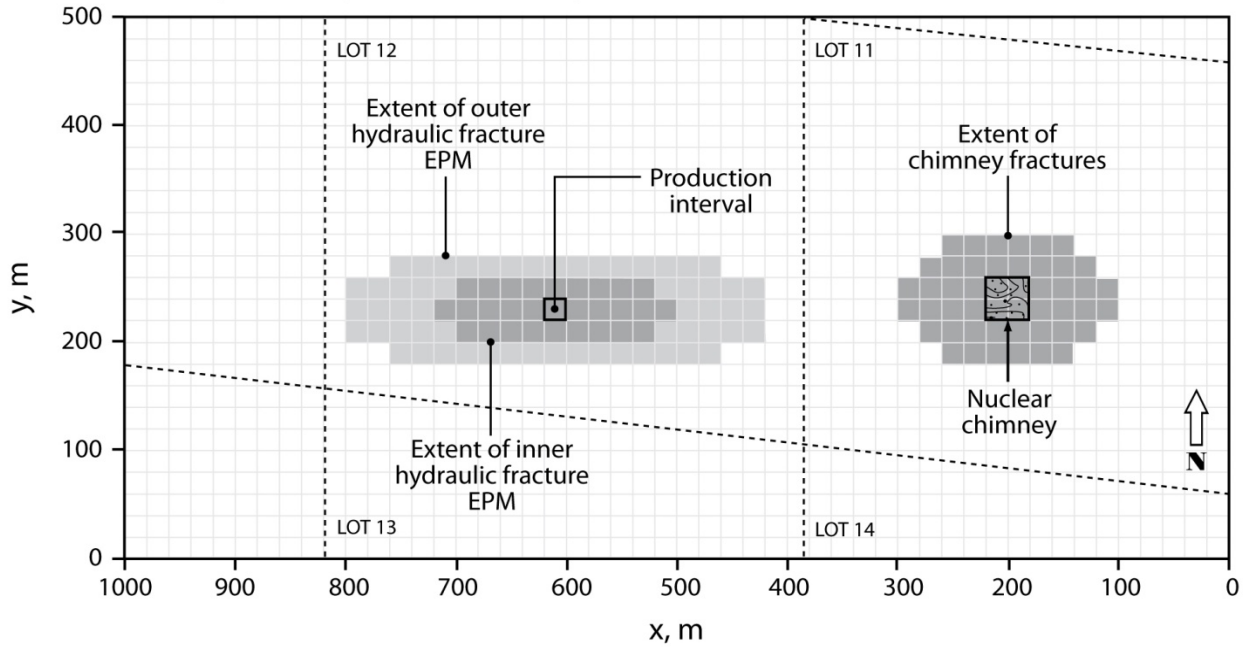

Figure 4. Plan view of the computational domain with nuclear chimney, chimney fractures, and inner and outer ellipsoidal fracture continua.

Relative Permeability and Capillary Pressure Functions

The relative permeability and capillary pressure functions for the chimney and fracture continua are updated to reflect more appropriate relationships of pressure and permeability as a function of liquid saturation for those rock types. The value for tortuosity, which describes the rate to which tritium diffusion is retarded due to the complex pathways particles travel through the porous rocks, is updated to a value determined from the analysis in Cooper *et al*. (2009).

In the Cooper *et al*. (2007) simulations, the same capillary pressure and relative permeability functions were assumed for all rock types. For the simulations reported here, more realistic functions are used for the nuclear chimney and shale rock types. Figure 5 shows these curves for the chimney and shale. The shale curves are based upon properties of clay from data provided in Carsel and Parrish (1988). Pertaining to the chimney, the maximum capillary pressure is small, < 40,000 Pa, as it is barely considered to be a porous medium due to the large blocks of rock that collapse into the nuclear cavity void to form the chimney. The result is that liquid moisture that is initially greater than the residual liquid saturation (the lowest saturation value attained at which point capillary forces are greater than gravity forces, resulting in no further drainage) quickly drains and puddles at the bottom of the chimney.

Table 1. Input data for the simulations. Values for which no references are given are not critical to the model results and are best estimates based upon nonspecific literature.

Gas Reservoir Parameters		
	Value	Source
Intrinsic permeability *x*-dir., sandstone, m^2	4×10^{-17}	From calibration, see text
Intrinsic permeability *y-, z*-dir., sandstone, m^2	4×10^{-18}	"
Intrinsic permeability, shale, m^2	10^{-20}	Randolph, 1983
Intrinsic permeability, nuclear chimney, m^2	10^{-12}	From calibration, see text
Intrinsic perm., explosion-related fracture epm, m^2	8.5×10^{-16}	"
Intrinsic perm., *x*-dir., inner ss epm, m^2	4×10^{-15}	sensitivity parameter
Intrinsic permeability *y*-, *z*-dir., inner ss epm, m^2	4×10^{-16}	"
Intrinsic perm., *x*-dir., outer ss epm, m^2	4×10^{-16}	"
Intrinsic permeability *y*-, *z*-dir., outer ss epm, m^2	4×10^{-17}	"
Intrinsic perm., *x*-dir., inner shale epm, m^2	4×10^{-16}	"
Intrinsic permeability *y*-, *z*-dir., inner shale epm, m^2	4×10^{-17}	"
Hydrofracture epm length, m	200 m	See text
Hydrofracture epm height, m	25 m	Cooper et al., 2007
Relative permeability	$K_l=S^4$	Corey, 1954
Capillary pressure curve	TRUST fit	Pruess *et al.,* 1999
Porosity, sandstone	0.03	Calibration, see text
Porosity, shale	0.07	Randolph, 1983
Porosity, nuclear chimney	0.25	Calibration, see text
Porosity, explosion-related fracture epm	0.06	"
Porosity, inner- outer-ss epm, inner shale epm	0.03	"
Rock grain density, kg m^{-3}	2,680	
Formation pressure (gas static), MPa	20 at base	Coffer *et al.,* 1971
Liquid saturation	0.5	Frank, 1971
Gas saturation	0.5	Frank, 1971
^3H radioactivity, liquid and gas, Ci	6941	Smith, 1971; AEC, 1972
Reservoir temp., ^oC	101	Smith, 1971
Diffusion coefficient, THO in methane, $m^2\ s^{-1}$	7.26×10^{-5}	Cussler, 1997
Diffusion coefficient, THO in liquid water, $m^2\ s^{-1}$	3.47×10^{-9}	Mills, 1973
Diffusion coefficient, CH_4 in liquid water, $m^2\ s^{-1}$	1.49×10^{-9}	Reid *et al*., 1987 (calculated)
Tortuosity	0.047	Cooper *et al*. (2009)
^3H half life, yr	12.26	Parrington *et al*., 1996
Rock grain specific heat, J kg^{-1}	1,000	
Thermal conductivity (unsaturated) of rocks, W m^{-1} ºC	2	

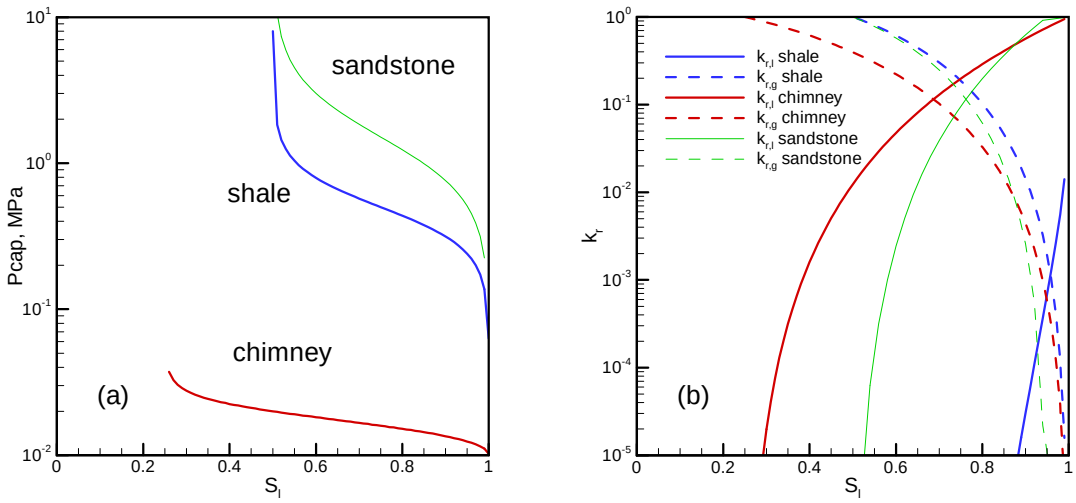

Figure 5. Capillary pressure (a), and relative permeability to liquid and gas (b) for the shale, chimney, and sandstone.

Tritiated Water Partitioning Between Liquid and Gas

Partitioning of tritiated water (THO) between the liquid and vapor phases is a critical process when considering vapor-phase migration of THO. In an environment where the gas phase velocity is much higher than the liquid phase, partitioning effectively becomes a significant retardation mechanism. When considering a decaying component such as tritium, retardation processes slow transport and allow tritium to decay to non-hazardous helium before significant migration.

Tritium partitioning between phases is implemented using a Henry's law formulation. Tritium exists as part of the water molecule, as THO (one atom of tritium and one atom of hydrogen) instead of the more-commonly form H_2O, and partitions between the gas and aqueous phases in accordance with Henry's law. Henry's law states that for dilute solutions in contact with a gas phase, the vapor pressure of the solute is proportional to its mole fraction in the solution. That is, the tendency for solute molecules to escape the aqueous phase is proportional to their mole fraction. We showed in the 2009 addendum that this same law can be applied to water molecules containing one tritium atom escaping a "solution" of nontritiated water. All that is required is to determine the value of the partitioning coefficient, as was done in the addendum.

The 2007 Rulison model report (page 53) used a trial-and-error method of estimating *HCRN1* by adjusting the *HCRN1* parameter value in TOUGH2 until the targeted tritium mass fraction in the gas phase was achieved. The resulting *HCRN1* was 9.65 x 10^{-8} Pa^{-1}. Ron Falta evaluated *HCRN1*, and through substitution allowed by the equilibrium partitioning derived a simple inverse relationship between *HCRN1* and the temperature-dependent water vapor pressure. At a temperature of 100 °C, Falta found *HCRN1* to be 9.9 x 10^{-6} Pa^{-1}. Falta confirmed his derivation with a test using TOUGH2, and also derived a dimensionless inverse Henry's constant consistent with the coefficient used by Smiles (1995) of 1.7 x 10^{-5} at 20 °C. Falta's work is recorded in the appendix of the 2009 Rulison addendum. Falta's derivation is evaluated for a variety of temperatures in a graph of the *HCRN1*-temperature relationship on page 5 of the addendum.

The analysis in the addendum establishes a firm theoretical basis for the appropriate *HCRN1* for the Rulison problem. Data collected during Rulison site activities in the 1970s provide the opportunity to use empirical data to estimate observed tritium partitioning and compare those observations to the theoretically based estimate for *HCRN1*. The relevant data are presented in the Project Rulison Final Operational Radioactivity Report Production Tests, dated February 1972, and published as report NVO-112, PNE-R-57. Gas from the chimney was brought to the surface during several pressure-test episodes. Measurements were made of the tritium concentration in "water in gas after the separator," "water vapor in gas after the bulk liquid traps," and "water removed by the separator." These data provide an opportunity to compare measurements of tritium in vapor and liquid to the partitioning calculations. Temperature data are available in the report entitled Project Rulison Post-Shot Well Test Data, undated, and published as PNE-R-52.

Consider measurements made at the end of the second production test, on December 20, 1970:

- C_v Tritium concentration in water vapor in gas after the bulk liquid traps = 3.74×10^5 pCi ml^{-1}
- C_l Tritium concentration in water removed by the separator = 5.11×10^5 pCi ml^{-1}

Temperatures measured at the wellhead and at the separator during the period when the samples were collected range from 103 to 105 °C. Bottom-hole temperature is reported as 222 to 223 °C for the same period.

First, we can evaluate the equilibrium assumption. The concentration of tritium condensed from the water vapor and in the liquid water are similar, indicating that tritium between the two phases is close to equilibration (note that the conversion to mass fraction from concentration is identical for the two concentrations, X_l^{THO} =3.53 x 10^{-10} and X_v^{THO}=2.58 x 10^{-10}, allowing comparison of the concentrations directly).

Next, we can consider the dimensionless partitioning coefficient used by Smiles:

$$H = \frac{C_g}{C_l} \tag{1}$$

C_l has been measured directly in the water removed by the separator, but we must calculate the concentration of tritiated water vapor as a portion of the total gas phase, C_g. Converting from volume to mass using the density of water of 1 g cc^{-1}, the concentration in the water vapor is 3.74×10^5 pCi g^{-1}. Using a saturated vapor density of 17.3 g-H_2O m^{-3}-air (for 20°C), there are 6.47×10^6 pCi m^{-3} of gas. Going back to ml, brings 6.47 pCi ml^{-1} of gas. Substituting into Smiles' equation gives an H of 1.27×10^{-5}. This compares to the value given by Smiles of 1.7×10^{-5}. If the more appropriate temperature of 100°C (saturated vapor density of 598 g/m^3) is used, the concentration is 2.24×10^8 pCi m^{-3} of gas, with an H of 4.4×10^{-4}, in contrast to approximately 6×10^{-4} (converting Falta's *HCRN1* of 9.869×10^{-6} Pa^{-1}).

Finally, we can consider Falta's *HCRN1* in units of Pa^{-1}:

$$HCRN1 = \frac{\omega_l^{THO}}{P_g^{THO}} \tag{2}$$

where ω_l^{THO} is the mole fraction of THO in liquid. Again, ω_l^{THO} was measured directly. The partial pressure of tritiated water vapor in the total gas (P_g^{THO}) can be calculated from the saturated vapor pressure of the water vapor (2334 Pa at 20 °C) and the tritium mole fraction in the vapor phase. This gives us the portion of the saturated vapor pressure attributable to tritiated vapor as 5.42 x 10^{-7} Pa. Substituting into Falta's equation gives a *HCRN1* of 5.55 x 10^{-4} Pa^{-1}, in contrast to his value of 4.3 x 10^{-4} Pa^{-1}. Considering a temperature of 100 °C (saturated vapor pressure of 101,325 Pa), the tritiated vapor pressure would be 2.35 x 10^{-5} Pa, and *HCRN1* would be 1.28 x 10^{-5} Pa^{-1}, very nearly Falta's value of 9.869 x 10^{-6} Pa^{-1}.

Uncertainty in this analysis comes principally from not knowing what temperature to use for the saturated vapor density, and equilibrium vapor saturation may also be in question for the dynamic conditions involved in the gas production and sampling processes. In addition, there is some, unquantified, uncertainty associated with the gas measurements themselves. The relationship between tritium in water vapor and tritium in separator water for the first, second, and third production tests is shown in Figure 6.

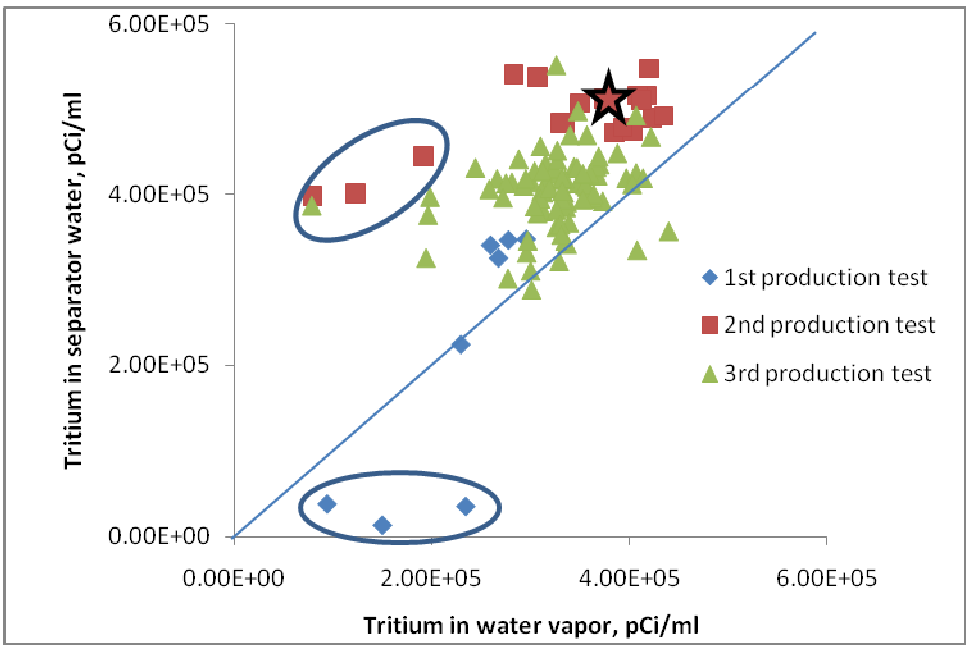

Figure 6. Measurements of tritiated water in liquid and vapor phases, measured during Rulison production testing. The circled areas show the first three samples from the first and second tests, which are clearly different than the subsequent samples and may represent initial sampling or analysis difficulties. The sample represented by a star is the one used in the calculations discussed in the text.

FLOW MODEL CALIBRATION

The accuracy of flow models of subsurface systems are generally assessed by comparing the pressures calculated by a model to measurements in the field. Calibration is the process of adjusting model input until computed values match the field values. Comparison of the reservoir pressures simulated by the original Rulison model during the gas production scenario indicated that pressure drawdown observed in gas wells producing from the lower Williams Fork

Formation were not being replicated in the model. Specifically, formation pressure at the production interval in the hypothetical well did not decrease as expected. Rather than speculate about pressure drawdown at a hypothetical well, the model is calibrated here to pressures observed during production testing at the Rulison site itself.

The models presented in the Cooper *et al*. (2007, 2009) reports are based upon permeability and porosity data collected from cores and production tests. A distribution of permeability and porosity values was then developed which resulted in the generation of 500 separate permeability and porosity fields for the computational domain. Five hundred simulations were then run, each with a different permeability and porosity realization, to develop a statistically based probability that tritium would reach the production well within 100 years following the nuclear detonation. For the simulations considered in this report, an improved method was developed to estimate permeability and porosity of the nuclear-generated fracture continuum and sandstone. The model was partly calibrated to data from a borehole (R-EX) that was drilled into the chimney in 1970. Three production tests were conducted on well R-EX between Oct. 4, 1970 and Sept. 27, 1971, to estimate the chimney size and to better characterize the amount of gas in place. The bottom hole pressure and flow rate data from the year-long series of production tests were used in the current study to inversely determine (or calibrate) values of permeability and porosity of the Williams Fork Formation. This was done on a single permeability realization with the ellipsoidal-shaped fracture zone around the chimney and a chimney temperature of 230 °C until the best fit was obtained; the parameters resulting in the best fit were then run with the other eleven permeability and porosity realizations. The formation properties were systematically changed in repeated simulations until the simulation correctly matched the history of actual production. Figure 7 compares the production test bottomhole pressures from the actual test with those of the simulation. The permeability (k_x in the east-west direction and $k_{y,z}$ in the north-south and vertical directions, respectively) and porosity (n) of the match are k_x=4 x10^{-17} m^2, $k_{y,z}$= 4 x 10^{-18} m^2, and n=0.03, respectively. These values are well within the parameter distributions used in the 2007 model. The k_x value is about an order of magnitude less than the mean value determined in the 2007 model while k_y and k_z are nearly the same as the mean values in the 2007 model. The mean permeabilities in Cooper *et al*. were k_x= 1.5 x 10^{-16} m^2, $k_{y,z}$ = 2.63 x 10^{-18} m^2, and the mean porosity was 0.0529. With this calibration, the uncertainty range in permeability and porosity can be reduced around the calibrated values. A simulation was also run with constant temperature throughout the domain to compare the effect of temperature on the resulting pressure field. The results show little difference in pressure response between the two simulations (Figure 7), which shows that with respect to pressure response, a chimney temperature of 230 °C has little effect on calibration.

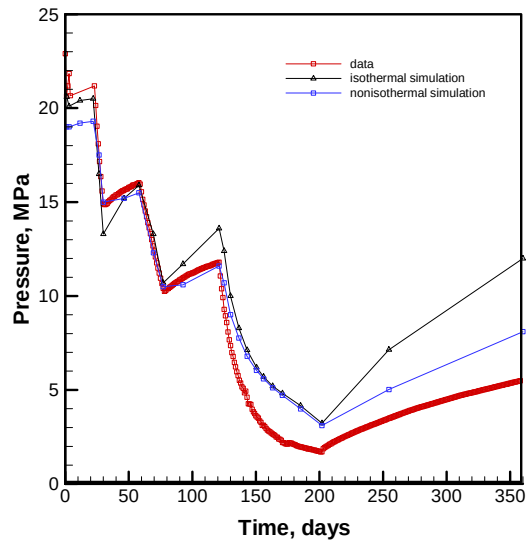

Figure 7. Simulated history match of pressure, for one permeability realization, compared to data from the 1970 production test.

In addition to permeability and porosity of the various rock types, the calibration procedure identified another area of improvement for the model. In the Cooper *et al*. (2007) report, gas production from the well was handled by prescribing a flow rate obtained by Presco, Inc. (written comm.). As noted previously, those simulations did not produce reasonable pressure fields around the production interval. Total pressure at the producing grid block never dropped below 19 MPa (the initial total pressure was 20 MPa at the domain bottom). Wells in the Rulison field typically produce against a well head pressure of around 2.5 MPa (400 psi). After the successful calibration, gas production is modeled by having the hypothetical well operate on deliverability against a 2.5 MPa flowing pressure at the production interval; in addition, a pressure equivalent to a static column of gas was added to the bottom hole flowing pressure. No allowances were made for pressure drop in the well. Mass production was modeled as

$$q_\beta = \frac{k_{r\beta}}{\mu_\beta} \rho_\beta \cdot \mathrm{PI} \cdot \left(P_\beta - P_{wb} \right) \tag{3}$$

where q_β is the flow rate of a phase (gas, in this case, $L^3\ t^{-1}$), $k_{r\beta}$ is the relative permeability to the phase [L^2], μ_β is the dynamic viscosity of the phase [$M\ L^{-1}\ t^{-1}$], ρ_β is fluid density of the phase [$M\ L^{-3}$], P_β is the phase pressure in the reservoir [$M\ L^{-1}\ t^{-2}$] and P_{wb} is the phase pressure at the wellbore. The productivity index, PI, is a factor that accounts for the fact that the wellbore does not consist of the entire (i.e., much larger) grid block, and is defined as

$$\left(\mathrm{PI}\right)_l = \frac{2\pi \left(k \Delta z_l \right)}{\ln\left(r_e / r_w \right) + s - \frac{1}{2}} \tag{4}$$

where k is the intrinsic permeability (m^2), Δz_l is the thickness of the production zone (5 m), r_e and r_w are the radii of the grid block and well, respectively, and s is a skin factor (assumed zero).

SUMMARY OF MODIFICATIONS TO THE RULISON FLOW AND TRANSPORT MODEL

The features and modifications described in the previous sections are implemented in an update to the Rulison flow and transport model. The computation domain, boundary and initial conditions are nearly the same as those presented in the previous two reports, with the following differences. The domain was lengthened to 1000 m in the horizontal *x*-direction to enable the model to handle longer hydraulic production fractures. The dimensions in the lateral *y*- and vertical *z*-directions remained the same, at 500 m and 400 m, respectively. In all figures, the detonation is 200 m from the right-hand (east) boundary, to allow for gas- and aqueous-phase diffusion in all directions. A 41-year period of diffusion follows the detonation (from 1969 to 2010), at which time gas production occurs from a hypothetical well located 201 m (666 ft) from the boundary between lots 11 and 12. This induces flow from east to west (right-to-left) in the figures, along the direction of the predominant fractures. The hydraulic and transport boundary conditions in the *y*-*z* planes at *x*=0 m and *x*=1000 m are prescribed total pressure (initialized as gas static) and zero concentration of tritium, respectively. Along the east-west (*x*-*z*) planes the hydraulic and transport boundary conditions are no flow and no tritium flux, respectively. The upper horizontal boundary conditions are no flow (i.e., impermeable) and no tritium flux, and the bottom boundary conditions are prescribed total pressure and zero concentration of tritium. The domain is of sufficient size as gas wells are produced on 10-acre spacings; a 20-acre square is 284 m per side and easily fits within the domain. This is important as actual gas wells are spaced such that drainage (pressure drawdown during production) occurs within the prescribed acreage.

The input values used in the simulations are presented in Table 1. In summary, the model discussed here differs from the 2007 model in the following manner:

- The tortuosity value is 0.047 (derived in the addendum), rather than a parameter that could be as low as 10^{-5} (as was used in the 2007 report)
- Tritium partitioning between the gas and aqueous phases is completely dependent upon temperature; temperature-dependent simulations were run in order to implement this feature
- A single value of sandstone permeability and porosity is used, rather than a distribution, based upon the calibration
- Gas production is simulated using a deliverability approach rather than prescribed flow
- Sandstone percentage is set at 40% rather than 49% of the domain
- Nuclear fracture and hydraulic fracture continua are simulated as having ellipsoidal shape in the horizontal plane rather than cylindrical, resulting in longer fracture lengths in the east-west direction
- The hydraulic fracture continua simulates fracturing of all rock within 100 m and an outer zone of increased permeability in only sandstone, rather than the single, smaller, increased-permeability zone in only sandstone simulated in the previous model
- Separate capillary pressure and relative permeability curves are used for sandstone, shale, hydraulic fractures, and the nuclear chimney

MODEL RESULTS

Results of Tritium Migration under Existing Conditions

The model was first run for a 41-yr period in the absence of any total pressure gradient (i.e., no horizontal pressure gradient and a gas-static initial condition). This forecasts the location and concentration of the "plume" of tritiated water vapor in the year 2010. Following an initial period of rapid diffusion through the nuclear-generated fractures and surrounding sandstone and shale, there was little transport of tritium. Figure 8 shows the mass fraction (a dimensionless concentration) field of tritiated vapor (X_g^{THO}) in five-year increments for a single realization; the other realizations resulted in nearly the same profiles. The moisture content in the chimney is high just after the start of the simulation, as liquid water drains downward, resulting in greater mass of tritium to exchange phases (into the gas) and the bell-shaped mass fraction profiles. The model results indicate that tritium has been limited to lot 11 since the nuclear detonation.

A simulation to investigate long-term transport in the absence of gas production is shown in Figure 9a. This simulation did not include advective flow and is an extension (to 75 yr) of the simulation presented in Figure 8. The results show that tritium is contained within lot 11 for the entire 75-year period. There is little change in tritium transport distance between 41 yrs (Figure 8) and 75 yr (Figure 9a) after the detonation because tritium diffusion is essentially balanced by radioactive decay, causing transport to reach pseudo-steady-state. The effect of decay is obvious in the diminishing concentration of tritium within the chimney at 75 years in comparison to 41 years. Another diffusion-only simulation is shown in Figure 9b, testing the sensitivity of diffusion to uncertainty in starting tritium mass. Bowen *et al*. (2001) indicate that estimates of residual tritium from underground nuclear tests have a wide range of uncertainty, from 1 to 300%, so the test used an initial mass fraction of tritiated water three times that which was used in all other simulations. A comparison between Figures 9a and 9b shows that the extent of tritium is nearly the same for the higher concentration, but that higher mass fractions occur within the tritium "plume" for equivalent times.

Results of Future Hypothetical Gas Production

After a 41-year period of tritium diffusion, a gas production well is included in each of the 12 simulations to determine the effect of a production-induced pressure gradient on tritium transport. A plot of the pressure field surrounding the gas production interval in the well after 30-years of production is shown in Figure 10. There are no publicly available data on pressure fields in production wells in any of the lots surrounding lot 11, but the pressure fields exhibit reasonable behavior, based upon experience with other gas wells in the area. The pressure field drops as low as 8 MPa (from a reservoir pressure of 20 MPa) at the production interval, and extends beyond the 200 m fracture EPM radius from the well in the east-west direction. In ten of the 12 simulations, appreciable pressure drop reaches from lot 12 to 40 m inside lot 11. As is shown below, the combination of weak pressure gradient and low tritium mass fraction never results in tritium reaching the well, or even migrating out of lot 11.

Figure 11 shows the rate of gas production of all 12 simulations producing against the specified borehole pressure. The exponential decline in production is realistically simulated, as the flow rates vary between 0.02 kg s^{-1} and 0.08 kg s^{-1} (90 MCFD and 360 MCFD) over the 30-yr period of production. Integration of the curves in Figure 11 shows that the total amount of gas produced over 30 years is between 1.1 and 2.6 billion cubic feet of gas (BCF) from the single production interval.

The mass fraction field of tritiated water vapor for each of the realizations, after 30 years of production, is shown in Figure 12. The different plume shapes result from the different heterogeneous permeability and porosity fields. Although the pressure drawdown reaches to within lot 11 in most of the simulations, tritium transport is only slightly enhanced, and in no case extends beyond lot 11.

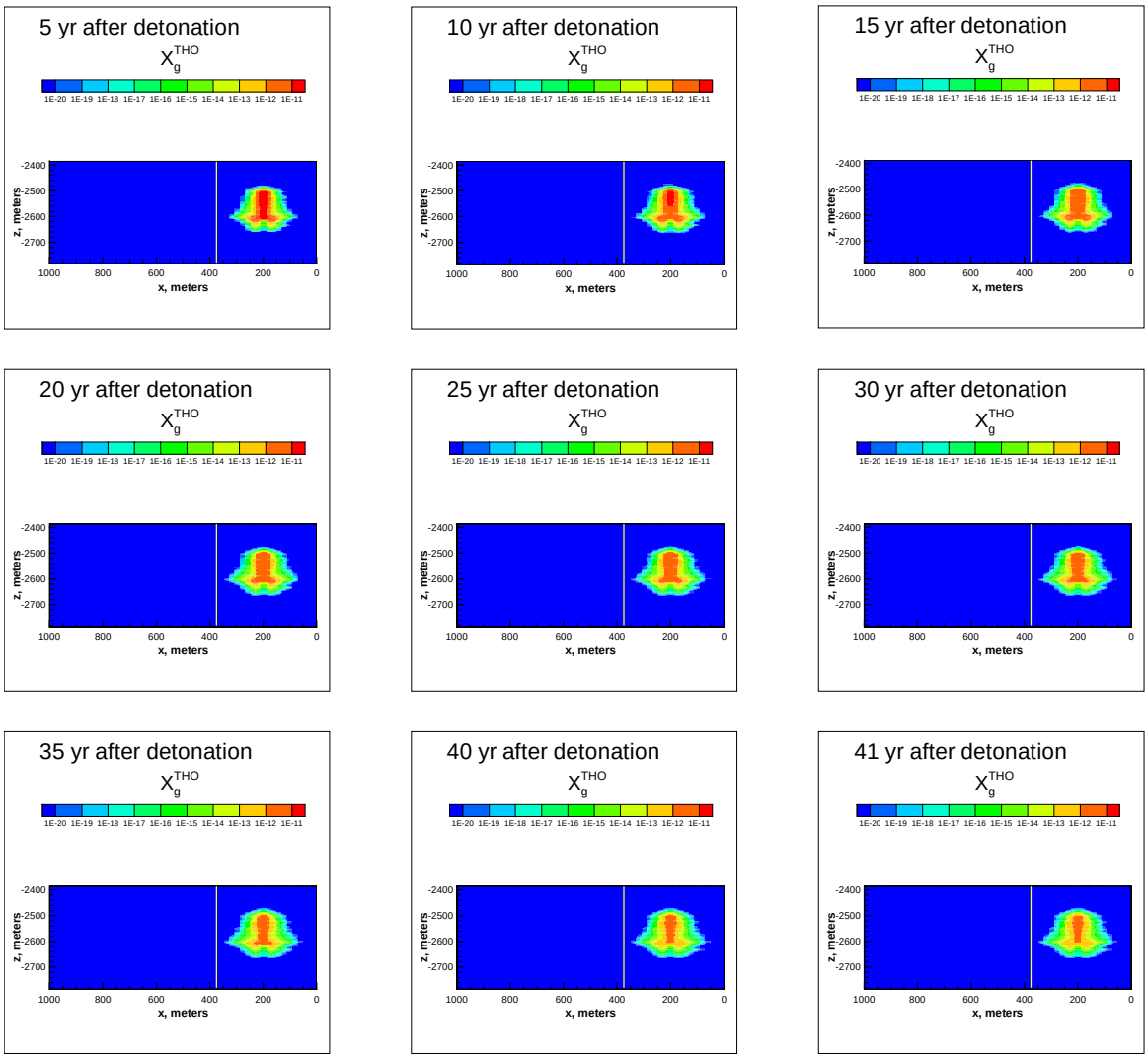

Figure 8. Mass fraction of tritiated water vapor in five-year increments for 41 years following the nuclear detonation for realization 1. Each pane shows a two-dimensional vertical east-west slice that cuts through the detonation point. Corresponding values in picocuries are 4 x 10^{10} picoCuries per liter (liquid water equivalent of condensed vapor) for X_g^{THO} =10^{-10} (the red end of the scale) to 4 pCi l^{-1} for X_g^{THO} =10^{-20} (the blue end of the scale). The vertical axis is depth below land surface, and the vertical yellow line depicts the boundary between lot 11 (to the right of the line) and lot 12.

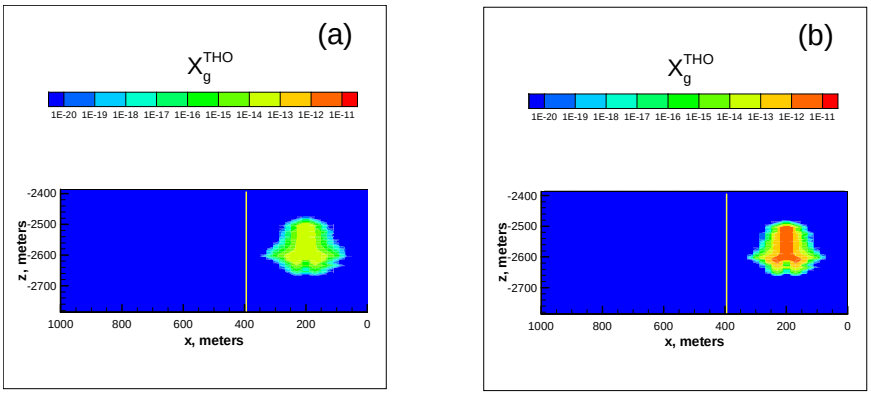

Figure 9. Tritiated water vapor 75 years after the nuclear detonation for (a) diffusion only (i.e., no gas production), and (b) for an initial condition three times the value used in the reference simulations (i.e., shown in Figure 8). The random permeability field is the same as that in Figure 8.

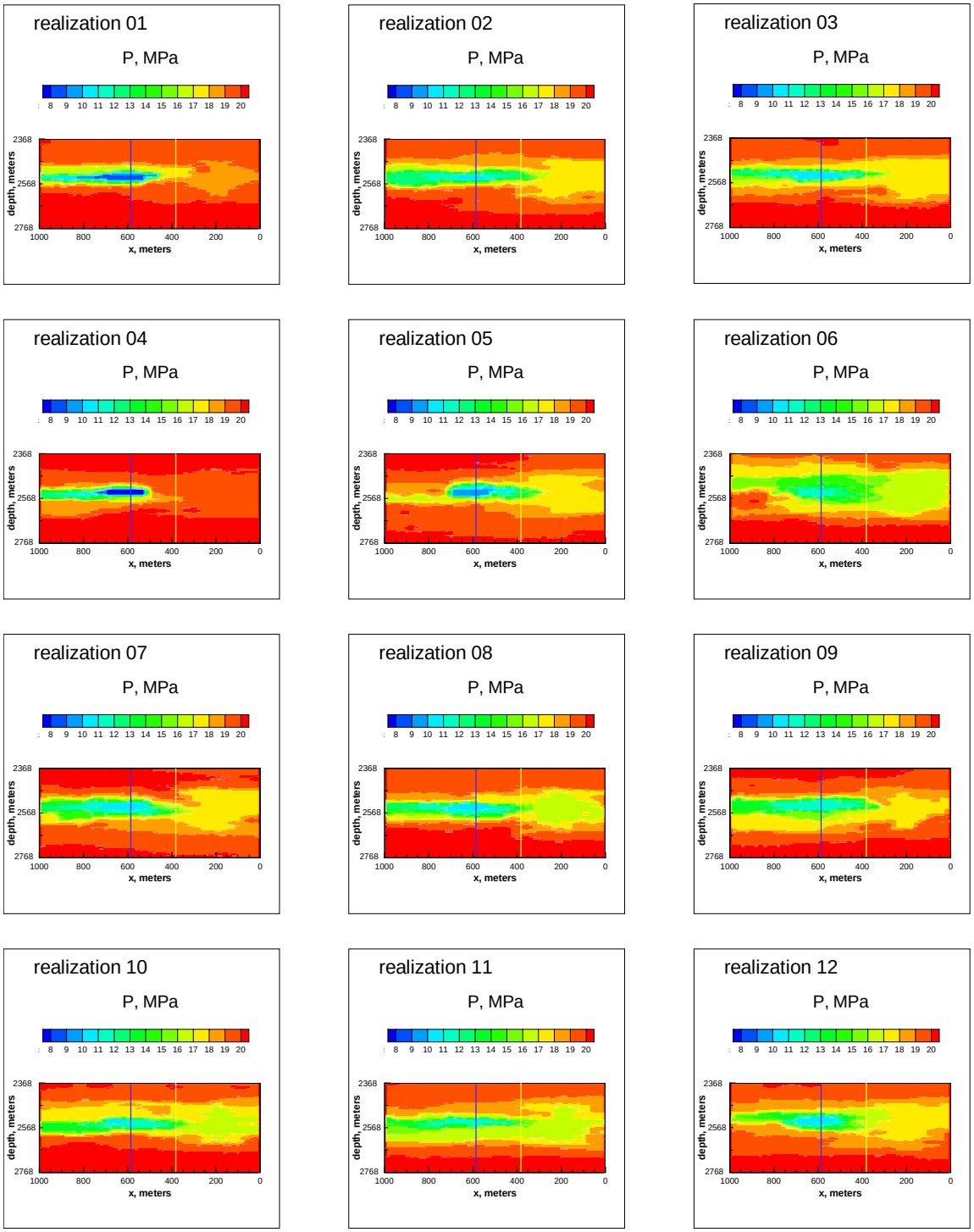

Figure 10. Total pressure field (in megapascals) after 30 years of gas production for all 12 permeability/porosity realizations. The vertical yellow line is the lot boundary and the vertical blue line is the location of the hypothetical production well.

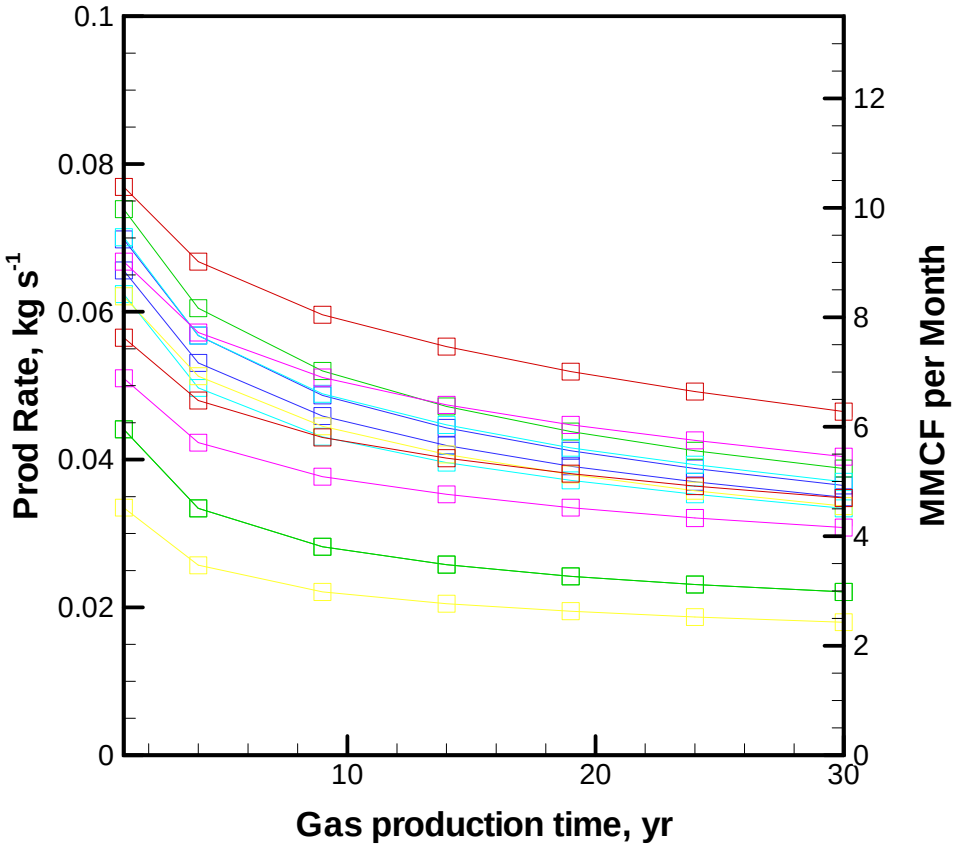

Figure 11. Gas production rate during 30-year period, between 41 and 71 years after the detonation, for all 12 permeability realizations. The right-hand axis is in thousand cubic feet of gas per month.

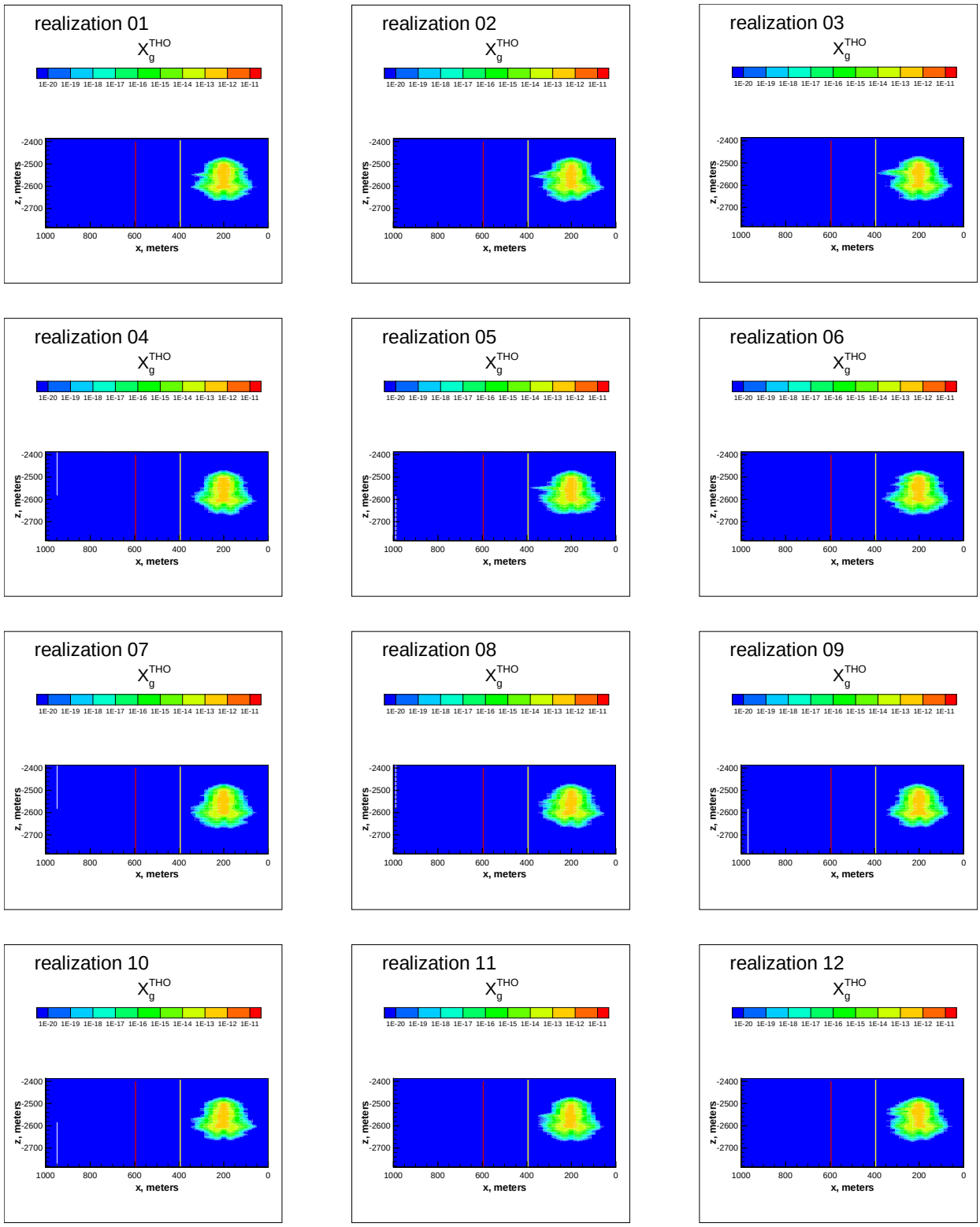

Figure 12. Mass fraction of tritiated water vapor after 30 years of gas production from the well, for all 12 realizations. The vertical axis is depth below land surface. The vertical yellow line is the boundary between lot 11 (to the right of the line) and 12, while the vertical red line shows the location of the hypothetical production well.

SUMMARY AND DISCUSSION

This report documents an updated computer model of subsurface tritium migration from a nuclear detonation conducted in 1969 in a gas producing reservoir located within the Parachute Field in west-central Colorado. The detonation was in the lower part of the Williams Fork Formation, a heterogeneous formation composed of sandstone and shale deposited in a fluvial environment. Details of the original model are presented in two previous documents (Cooper *et al*., 2007, 2009); this report explains modifications to the model and the impact on simulated tritium transport.

The framework for the computer simulations are individual random fields of sandstone and shale. Unlike the models in the previous reports, a single value for sandstone permeability and porosity, determined from calibration to a production test of a well drilled into the chimney in the early 1970s, was used for all simulations. This differed from the previous work where both the sandstone/shale lithology and sandstone permeabilities were treated as random variables. In addition, the percentage of sandstone that was assigned to develop the sandstone and shale fields was reduced from 49 to 40%, based on recent geologic data from near the Rulison test.

Within the geologic framework, the equivalent porous medium depiction of the nuclear-generated fractures around the nuclear chimney, and hydraulic fractures hypothesized around a future production well is changed from previous models. The current model elongates fracture lengths in the direction of principal regional stress, along the east-west direction. The impact of the hydraulic fractures on the flow field, and their length, was also significantly enhanced in the updated simulations.

Several other changes were made to the model based upon a sensitivity study reported in Cooper *et al*. (2009). The TOUGH2 code was modified such that the inverse Henry's law constant changes throughout the simulation as a function of the local temperature within a grid block, resulting in more accurate partitioning of tritium between the aqueous and gas phases. The other important change is that the tortuosity value is 0.047, which enhances gas diffusion in comparison to the much lower values calculated in the Cooper *et al*. (2007) report.

The simulation results are composed of two parts. The first part is a 41-year period of diffusion (from the year of the detonation in 1969 to 2010) and reflects the best estimate of the current location and amount of tritium that has migrated since the detonation. The results suggest that tritium is confined to lot 11 for all permeability fields. A single simulation was carried out to 75 years in which tritium transport reached a pseudo steady state and remained within lot 11. The diffusion distance was not sensitive to a three-fold increase in the amount of tritium mass for the one realization tested. Within the limitations of the model, it can be inferred that at the present time, tritium is most likely confined to within lot 11 and if undisturbed will likely remain there in the future.

The second part of the model addresses gas production from an interval within a hypothetical gas well located in lot 12, 201 m (660 ft) from the boundary between lots 11 and 12. The production period is assumed to occur between the years 2010 and 2040, against a continuous borehole pressure of 2.5 MPa (400 psi). The results show that tritium is confined within lot 11 in all of the simulations, as the combination of weak pressure gradient and low tritium mass fraction do not significantly enhance transport. The current model predicts that tritium will be confined to lot 11in all 12 simulations. The previous model results reported by Cooper *et al.* (2007) and (2009) predicted tritium would reach a production well in fewer than

five percent of the 500 realizations. The primary reason the current simulations forecast no migration beyond the lot 11 boundary appears to be due to partitioning tritium between the aqueous and gas phases as a function of the local temperature. Partitioning in the previous models used a single partitioning coefficient throughout the entire computational domain, resulting in overestimated tritium transport in the reservoir beyond the nuclear chimney. These results show less tritium transport throughout the reservoir even though the mean sandstone permeability has been increased with respect to previous simulations, longer fracture lengths are simulated, and a lower gas pressure (2.5 MPa) is prescribed during the production phase.

The Rulison tritium transport model reported here is considered to be superior to previous versions in that it better simulates critical processes, such as tritium partitioning and diffusion, and more conservatively depicts uncertain future conditions, such as hydraulic fracture length. In the process of conducting the previous and current model simulations, a wide range in parameter values has been explored and multiple techniques implemented for simulating the complex multiphase flow and transport conditions. The forecast of limited transport has remained robust despite the many differences between conceptual and numerical aspects of these models. Nonetheless, new data from the subsurface near the Rulison test, changes in reservoir development practices, or advancements in the theory and application of unsaturated flow and transport simulation could suggest additional simulations of value to site stewardship.

REFERENCES

Bowen, S.M., D.L. Finnegan, J.L. Thompson, C.M. Miller, P.L. Baca, L.F. Olivas, C.G. Geoffrion, D.K. Smith, W. Goishi, B.K. Esser, J.W. Meadows, N. Namboodiri, and J.F. Wild, 2001. Nevada Test Site Radionuclide Inventory, 1951-1992. Los Alamos National Laboratory report LA-13859-MS, 28p.

Carle, S.F., 1999. T-PROGS: Transition Probability Geostatistical Software, Version 2.1, University of California, Davis.

Carsel R.F., and R.S. Parrish, 1988. Developing joint probability distributions of soil water retention characteristics, *Water Resour. Res.,* 24(5): 755-769.

Cole, R.D. and S.P. Cumella, 2005. Sand-Body Architecture in the Lower Williams Fork Formation (Upper Cretaceous), Coal Canyon, Colorado, with Comparison to the Piceance Basin Subsurface. The Mountain Geologist, Vol. 42, No. 3, p.85-107.

Corey, A.T., 1954. The interrelation between gas and oil relative permeabilities. *Producer's Monthly*, XlX(1): 38-44.

Cooper, C.A., Ye, M., and J.B. Chapman, 2007. Tritium Transport at the Rulison Site, a Nuclear-Stimulated Low-Permeability Natural Gas Reservoir, Desert Research Institute Report no. 45224, 102 pp. *Same as* U.S. Department of Energy (DOE) Office of Legacy Management, 2007. DOE/NV/13609-54, DOE M/1522 2007.

Cooper, C.A., Ye, M., and J.B. Chapman, 2009, Addendum: Tritium Transport at the Rulison Site, a Nuclear-Stimulated Low-Permeability Natural Gas Reservoir. Letter Report.

Cussler, E.L., 1997. Diffusion Mass Transfer in Fluid Systems. 2nd edition, Cambridge University Press, 580 pp.

Mills, R., 1973. Self-diffusion in normal and heavy water in the range 1-45º. *J. Physical Chem.*, 77(5): 685-688.

Parrington, J.R., H.D. Knox, S.L. Breneman, E.M. Baum and F. Feiner, 1996. Nuclides and Isotopes. 15th Edition. General Electric Co., San Jose, CA, 64p.

Randolph, P.L., 1983. Porosity and permeability of Mesaverde sandstone core from the U.S. DOE Multiwell Experiment, Garfield County, Colorado. Proceedings paper SPE 11765 presented at the 1983 SPE/DOE Symposium on Low Permeability Gas Reservoirs, Denver, CO, March 4-6, 1983, pp.449-460.

Pruess, K., C. Oldenburg and G. Moridis, 1999. TOUGH2 User's Guide, Version 2.0. Lawrence Berkeley Laboratory Report LBNL-43134, Berkeley, CA.

Reid, R.C., J.M. Prausnitz, and B.E. Poling, 1987. The Properties of Gases and Liquids, McGraw Hill, 741 pp.

Reynolds, M.J., B.G. Bray, and R.L. Mann, 1970. Project Rulison: A Status Report. Society of Petroleum Engineers paper SPE 3191, proceedings paper presented at the 1970 Eastern Regional Meeting, Pittsburgh, PA, 16p.

Rogers, L. and M.R. Reynolds, Jr., 1972. Summary of Project Rulison. Unnumbered report prepared by El Paso Natural Gas and Austral Oil Company, in U.S. DOE/NV Technical Information Resource Center, 6p.

Smiles, D.E., Gardner, W.R., and R.K. Schulz, 1995. Diffusion of tritium in arid disposal sites, *Water Resour. Res*., 31(6): 1483-1488.

Smith, C.F. Jr., 1971. Gas analysis results for Project Rulison production testing samples. Lawrence Livermore Laboratory report UCRL-51153, 25p.